

# Radiation-balanced silica fiber laser

J. KNALL,<sup>1,\*</sup> M. ENGHOLM,<sup>2</sup> T. BOILARD,<sup>3</sup> M. BERNIER,<sup>3</sup> P.-B. VIGNERON,<sup>1</sup> N. YU,<sup>4</sup> P. D. DRAGIC,<sup>4</sup> J. BALLATO,<sup>5</sup> AND M. J. F. DIGONNET<sup>1</sup>

<sup>1</sup>Edward L. Ginzton Laboratory, Stanford University, Stanford, California 94305, USA

<sup>2</sup>Division of Electronics Design, Mid Sweden University, SE-85170 Sundsvall, Sweden

<sup>3</sup>Centre d'optique, photonique et laser (COPL), Université Laval, Québec, Québec G1V 0A6, Canada

<sup>4</sup>Department of Electrical and Computer Engineering, University of Illinois at Urbana-Champaign, Urbana, Illinois 61801, USA

<sup>5</sup>Department of Materials Science and Engineering, Clemson University, Clemson, South Carolina 29631, USA

\*Corresponding author: JennyKnall@Stanford.edu

Received 15 March 2021; accepted 3 May 2021 (Doc. ID 425115); published 1 June 2021

**In optically pumped lasers, heat generated by the quantum defect causes detrimental fluctuations in the output mode, frequency, and power. Common heat-mitigation techniques use bulky mechanical coolers that introduce vibrations, leading to laser frequency and amplitude noise. Here, we present a radiation-balanced fiber laser, optically cooled by anti-Stokes fluorescence (ASF). The gain medium is a silica fiber with a 21- $\mu\text{m}$ -diameter core doped with 2.06 wt. %  $\text{Yb}^{3+}$  and co-doped with  $\text{Al}_2\text{O}_3$  and F- to reduce concentration quenching. The laser was core-pumped at 1040 nm to create both gain at 1065 nm and ASF cooling at atmospheric pressure. We demonstrate a maximum output power of 114 mW with a slope efficiency of 41% while maintaining near-zero average temperature change. This result could enable the development of fiber lasers with unprecedented coherence and stability.** © 2021

Optical Society of America under the terms of the OSA Open Access Publishing Agreement

<https://doi.org/10.1364/OPTICA.425115>

Anti-Stokes fluorescence (ASF) cooling is a fully optical form of cooling, in which the host is pumped at a photon energy that is lower than the average photon energy of the spontaneous emission [1]. The fluorescence extracts energy from the system in an amount proportional to the average energy difference between the pump and fluorescence photons. ASF cooling is a broadly accepted concept that was first proposed, to the best of our knowledge, in 1929 [2] and demonstrated for the first time, to the best of our knowledge, in 1995 using a bulk sample of  $\text{Yb}:\text{ZBLAN}$  [3]. One of its primary applications is radiation-balanced lasers, a device in which the waste heat generated by the lasing process is negated by cooling induced by ASF [4]. This technique would eliminate the need for conventional heat-removal solutions such as forced-air, water, or thermoelectric cooling, which induce vibrations and/or temperature gradients within the laser—deleterious affects that result in modal and frequency fluctuations in the laser output. For fiber lasers, it is difficult to achieve perfectly radiation-balanced operation at every point along the gain fiber. Nevertheless, using ASF cooling to achieve zero average temperature change along the length will significantly reduce the temperature deviation at each point and go a long way toward improving the output

beam quality. Furthermore, the fiber can be strategically coiled to homogenize the temperature along its length [5].

In the past 25 years, there have been numerous demonstrations of ASF cooling in rare-earth-doped crystals and exotic hosts like fluorides [6]. Cryogenic temperatures have even been achieved in Yb-doped crystals placed in a vacuum to reduce the heat load due to air convection [6]. Bulk radiation-balanced lasers have also been reported in highly doped Yb:YAG [4,7]. However, until recently, cooling in silica remained elusive, precluding the application of ASF cooling from the most ubiquitous of all fiber materials.

The primary obstacle that prevented cooling in communication-grade silica was concentration quenching, a mechanism in which energy is transferred from an active rare-earth ion to an impurity, then relaxes to the ground state non-radiatively and generates heat [8]. The probability of quenching increases with ion concentration, thereby limiting the number of heat engines that can be doped into a given volume. The susceptibility of a particular host to quenching can be quantified by its critical quenching concentration, the concentration for which the mean distance between ions is such that the probability of quenching equals the probability of spontaneous emission. The critical concentration for  $\text{Yb}^{3+}$  is typically one order of magnitude lower in silica than in crystals or fluoride hosts [9,10]. This is due to a combination of factors, including the comparatively low solubility of  $\text{Yb}_2\text{O}_3$  in silica, which results in the formation of Yb clusters [11]. To achieve cooling in silica, it was critical to develop a glass composition and a fabrication protocol that addressed these issues.

This bottleneck was finally solved a year ago with reports of cooling in Yb-doped silica fiber [12] and fiber preform [13]. In both cases, the glass compositions were designed to support high concentrations of Yb with little quenching. For the silica fiber, this resulted in a critical quenching concentration 16 times larger than the highest value reported for Yb-doped silica, and comparable to values reported for Yb-doped ZBLAN, enabling the fiber to be doped with 2.06 wt. % Yb. This was achieved by co-doping the core with alumina to shift the immiscibility region to higher sesquioxide concentrations. This reduced the tendency for Yb clustering and, hence, quenching. The fiber was also co-doped with fluorine to dehydrate the glass and reduce  $\text{OH}^-$  impurities, which not only decreased the probability of quenching but also minimized heating due to direct absorption of the pump power. Care was also taken



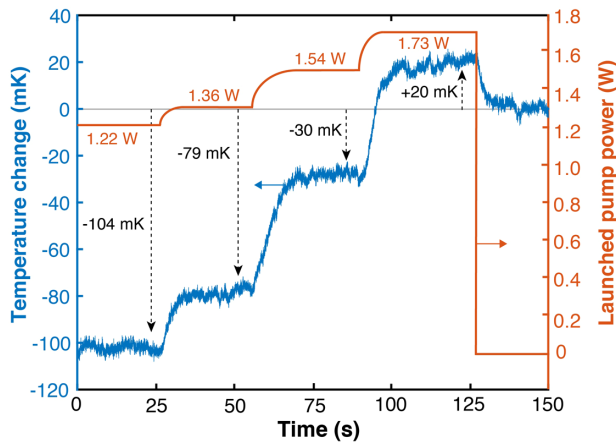


**Fig. 2.** Temporal trace of the temperature change recorded 19 cm from the output end of the Yb-doped silica fiber, core-pumped at four powers of 1040 nm light, represented pictorially by the red curve.

fiber), and the output of the laser was monitored with a power meter. The measurement started ( $t = 0$  s) once the output power stabilized ( $\sim 2$  min after the pump was turned on). At this time, the fiber temperature was  $-104$  mK below room temperature. The pump was left at 1.22 W for  $\sim 25$  s, then slowly turned up to the next power (1.36 W). This induced a slight heating of the fiber to a new steady-state value. This procedure was repeated for the remaining two pump powers (1.54 W and 1.73 W). After the fiber temperature reached a steady state for the highest power, the pump was abruptly turned off, and the fiber equalized to room temperature. The temperature change induced by each pump power was defined as the average difference between the last 5 s when the pump was turned off and the 5 s prior to changing the pump power. Each measurement was repeated three times and averaged.

The fiber laser output power at 1065 nm was measured as a function of launched pump power (blue crosses in Fig. 3), which was measured upon completion of the experiments using a cut-back method. The laser output was in the fundamental ( $\text{TEM}_{00}$ ) mode, since the higher-order modes were filtered out by the SMF-28 and HI-1060 fibers spliced to the output of the gain fiber. This filtering caused only slight fluctuations in the output power ( $\sim 5\%$ ) due to variations in the amount of power coupled to the higher-order modes along the Yb-doped fiber. As expected, the output power increased linearly once the threshold pump power was reached ( $\sim 1.07$  W).

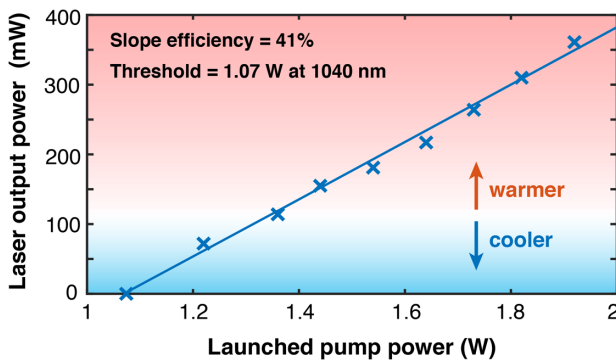


**Fig. 3.** Laser output power measured as a function of the launched pump power, along with a linear fit. The color gradient is a pictorial representation of the average temperature change along the length of the gain fiber.

The data was fit to a model of the RBFL described in [21]. All of the fiber parameter values needed for these simulations were either measured directly or inferred from fits to independent cooling and absorption measurements, as described in [10]. The FBG reflectivities were also measured. The only fitting parameters were the losses of the four splices to the SMF-28 fibers. The total round-trip loss [in decibels (dB)] of the two splices at the input of the Yb-doped fiber is defined as  $\alpha_{\text{in}}$ ; the corresponding quantity at the output end is  $\alpha_{\text{out}}$ . The output loss is further broken down into a forward propagating loss  $\alpha_{\text{out, fw}}$  and a backward propagating loss  $\alpha_{\text{out, bw}}$ , so that  $\alpha_{\text{out, fw}} + \alpha_{\text{out, bw}} = \alpha_{\text{out}}$ .  $\alpha_{\text{out, fw}}$  directly affects the laser output power as well as the residual pump power and needs to be fitted independently from  $\alpha_{\text{out, bw}}$ . Since the splices at both ends of the Yb-doped fiber are nominally identical,  $\alpha_{\text{in}}$  and  $\alpha_{\text{out}}$  were assumed to be equal. Completing the fit resulted in fitted values of  $\alpha_{\text{in}} = \alpha_{\text{out}} = 4.8$  dB and  $\alpha_{\text{out, fw}} = 2.4$  dB. These relatively high losses are in agreement with expectations. The calculated spatial overlap integral between the fundamental modes of the HI-1060 fiber and the SMF-28 fiber gives 0.27 dB of single-pass loss. Between the SMF-28 fiber and the Yb-doped fiber, this calculation gives 1.9 dB of loss. In total, the calculated round-trip loss for the two splices is 4.4 dB (compared to the fitted value of 4.8 dB). The extra 0.4 dB of loss can be reasonably attributed to (1) coupling to higher-order modes in the Yb-doped fiber, which results in an additional loss when these modes are filtered out at the splice to the SMF-28 fiber (but not in the other direction), and/or (2) core misalignment at the splices. From this fit, the threshold pump power was calculated to be 1.07 W. The slope efficiency was 41%, about half as much as typical commercial silica fiber lasers. The threshold and slope are in excellent agreement with the experimental data (see Fig. 3). In future iterations, the slope efficiency and the threshold can be significantly improved by eliminating the splice losses associated with  $\alpha_{\text{out, fw}}$ .

The temperature change along the 2.64 m fiber laser was measured for four different pump powers (Fig. 4). This resulted in the same general trend for all four powers. The fiber was the warmest at the input end and cooled monotonically along its length. For the lowest pump power (1.22 W), this resulted in a transition to negative temperature changes  $\sim 1$  m from the input end. Increasing the pump power caused this transition to occur further along the fiber, ultimately never occurring for the highest pump power (1.73 W). Three mechanisms contribute to heating at the input end. First, the pump power in this region exceeds the power that produces maximum cooling, which is calculated to be  $\sim 420$  mW for this

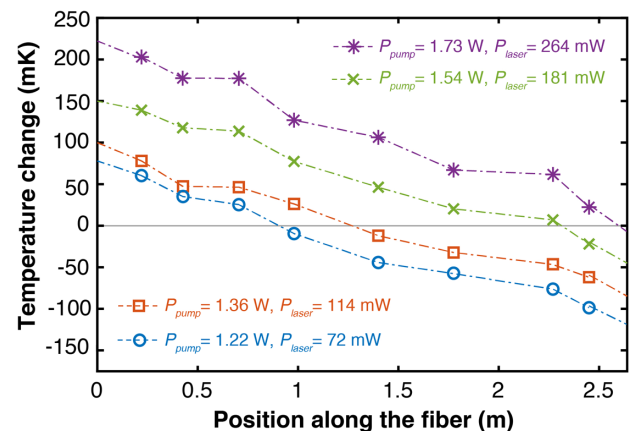


**Fig. 4.** Average measured temperature change at eight locations along a 2.64 m silica fiber laser for four different output powers at 1065 nm.

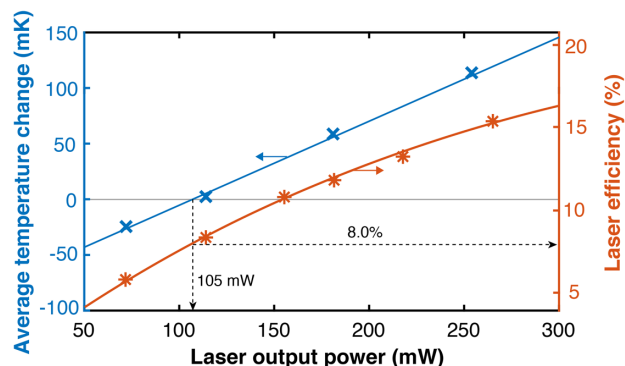


**Fig. 5.** Average temperature change along the fiber laser and the optical-to-optical laser efficiency, both measured as a function of laser output power, along with their associated fits.

fiber (see [17] for a physical explanation). Second, the higher pump power corresponds to greater signal amplification, which results in the generation of more Stokes phonons (more heating). Third, this is also where the intra-cavity signal power is the greatest and, therefore, where the depletion of the excited-state population is the highest (less cooling). Further along the fiber, as the pump power is attenuated, and the signal amplification saturates, these heating effects are lessened, and ASF cooling dominates. The dashed segments in Fig. 4 are interpolations of the eight temperature measurements taken for each output power. Integrating under each curve and dividing by the length of the fiber (2.64 m) gives an approximation for the average temperature change along the length of the fiber laser. For the 72 mW laser, this calculation yields an average temperature change of  $-24.4$  mK, indicating that more output power needs to be extracted to achieve radiation-balanced operation. The latter was very nearly achieved with the 114 mW laser, whose average temperature was calculated to be only 2.5 mK above room temperature (which is within the error of the sensor).

As expected, the average temperature change continued to increase linearly with output power, resulting in 58.8 mK for 181 mW and 113.8 mK for 264 mW. The blue crosses in Fig. 5 show these averages plotted as a function of laser output power, along with a linear fit (solid blue curve). Figure 5 also shows the optical-to-optical efficiency of the laser, calculated from the data in Fig. 3 by dividing the laser output power by the launched pump power (red asterisks and curve). From the curves, the laser output power associated with zero average temperature change is calculated to be 105 mW, and the associated optical-to-optical efficiency is 8.0%.

For the first time, to the best of our knowledge, a RBFL is demonstrated. The gain medium was a highly doped Yb silica fiber materially tailored to significantly reduce sources of non-radiative relaxation, including concentration quenching and the parasitic effects of  $\text{OH}^-$  and  $\text{Yb}^{2+}$  species. Pumped at 1040 nm to strike a near-optimum compromise between cooling and gain, the

1065 nm fiber laser had a threshold power of 1.07 W and a slope of efficiency of 41%, which was limited in part by avoidable splice losses. At an output power of 114 mW, the 2.64 m Yb-doped fiber laser had an average temperature within 3 mK of room temperature. This work launches a new class of fiber lasers with improved stability.

**Funding.** Air Force Office of Scientific Research (FA9550-16-1-0383); Natural Sciences and Engineering Research Council of Canada (RGPIN-2016-05877).

**Disclosures.** The authors declare no conflicts of interest.

**Data Availability.** Data underlying the results presented in this paper are not publicly available at this time but may be obtained from the authors upon reasonable request.

## REFERENCES

1. R. Epstein and M. Sheik-Bahae, *Optical Refrigeration: Science and Applications of Laser Cooling of Solids* (Wiley, 2009).
2. P. Pringsheim, *Z. Phys.* **57**, 739 (1929).
3. R. I. Epstein, M. I. Buchwald, B. C. Edwards, T. R. Gosnell, and C. E. Mungan, *Nature* **377**, 500 (1995).
4. S. Bowman, S. P. O'Connor, S. Biswal, N. J. Condon, and A. Rosenberg, *IEEE J. Quantum Electron.* **46**, 1076 (2010).
5. J. Knall and M. J. F. Dignonet, "Anti-Stokes-fluorescence-cooled fiber-based gain element," U.S. patent 10,790,633 (February, 20, 2020).
6. D. V. Seletskiy, R. Epstein, and M. Sheik-Bahae, *Rep. Prog. Phys.* **79**, 96401 (2016).
7. Z. Yang, J. Meng, A. R. Albrecht, and M. Sheik-Bahae, *Opt. Express* **27**, 1392 (2019).
8. F. Auzel, G. Baldacchini, L. Laversenne, and G. Boulon, *Opt. Mater.* **24**, 103 (2003).
9. P. Barua, E. H. Sekiya, K. Saito, and A. J. Ikushima, *J. Non-Cryst. Solids* **354**, 4760 (2008).
10. J. Knall, A. Arora, M. Bernier, S. Cozic, and M. J. F. Dignonet, *Opt. Lett.* **44**, 2338 (2019).
11. J. Ballato and P. Dragic, *J. Dir. Energy* **6**, 175 (2017).
12. J. Knall, P. B. Vigneron, M. Engholm, P. Dragic, N. Yu, J. Ballato, M. Bernier, and M. J. F. Dignonet, *Opt. Lett.* **45**, 1092 (2020).
13. E. Mobini, S. Rostami, M. Peysokhan, A. Albrecht, S. Kuhn, S. Hein, C. Hupel, J. Nold, N. Haarlamert, T. Schreiber, R. Eberhardt, A. Tünnermann, M. Sheik-Bahae, and A. Mafi, *Commun. Phys.* **3**, 1 (2020).
14. J. Kirchhof, S. Unger, A. Schwuchow, S. Grimm, and V. Reichel, *J. Non-Cryst. Solids* **352**, 2399 (2006).
15. M. Peysokhan, S. Rostami, E. Mobini, A. Albrecht, S. Kuhn, S. Hein, C. Hupel, J. Nold, N. Haarlamert, T. Schreiber, R. Eberhardt, A. Tünnermann, M. Sheik-Bahae, and A. Mafi, *ACS Omega* **6**, 8376 (2021).
16. J. Knall, M. Engholm, J. Ballato, P. Dragic, N. Yu, and M. J. F. Dignonet, *Opt. Lett.* **45**, 4020 (2020).
17. J. Knall, M. Engholm, T. Boilard, M. Bernier, and M. J. F. Dignonet, arXiv:2103.02698 (2021).
18. J. Knall, M. Esmaeelpour, and M. J. F. Dignonet, *J. Lightwave Technol.* **36**, 4752 (2018).
19. A. Arora, M. Esmaeelpour, M. Bernier, and M. J. F. Dignonet, *Opt. Lett.* **43**, 3337 (2018).
20. M. K. Davis and M. J. F. Dignonet, *J. Lightwave Technol.* **16**, 1013 (1998).
21. J. Knall and M. J. F. Dignonet, *J. Lightwave Technol.* **39**, 2497 (2020).